High-order harmonic generation in solid C_{60}

G. P. Zhang and Y. H. Bai

Phys. Rev. B **101**, 081412 — Published 26 February 2020

DOI: 10.1103/PhysRevB.101.081412

High-order harmonic generation in solid C_{60}

G. P. Zhang*

Department of Physics, Indiana State University, Terre Haute, Indiana 47809, USA

Y. H. Bai

Office of Information Technology, Indiana State University, Terre Haute, Indiana 47809, USA

(Dated: February 13, 2020)

Abstract

High harmonic generation (HHG) has unleashed the power of strong laser physics in solids. Here we investigate HHG from a large system, solid C_{60}, with 240 valence electrons engaging harmonic generation at each crystal momentum, the first of this kind. We employ the density functional theory and the time-dependent Liouville equation of the density matrix to compute HHG signals. We find that under a moderately strong laser pulse, HHG signals reach 15th order, consistent with the experimental results from C_{60} plasma. The helicity dependence in solid C_{60} is weak, due to the high symmetry. In contrast to the general belief, HHG is unsuitable for band structure mapping in C_{60}. However, we find a window of opportunity using a long wavelength, where harmonics are generated through multiple-photon excitation. In particular, the 5th order harmonic energies closely follow the transition energy dispersion between the valence and conduction bands. This finding is expected to motivate future experimental investigations.

PACS numbers: 42.65.Ky, 78.66.Tr

Keywords:

The discovery of Buckminsterfullerene [1] represents an era of nanoscience and nanotechonology revolution. Solid C_{60} is a van der Waals molecular crystal [2]. Once it is doped with potassium atoms, K_3C_{60} is a superconductor with transition temperature at 18 K [3], which can be modulated optically [4]. A single C_{60} molecule has the highest possible point group symmetry of I_h, among the most symmetric molecules ever discovered. Sixty carbon atoms form 20 hexagons and 12 pentagons, with 60 double bonds of 1.46 Å between hexagons and 30 single bonds of 1.40 Å between the pentagons and hexagons. These bonds support a carbon cage of diameter 7.1 Å. A mixture of sp^2-sp^3 bond is distinctively different from those found in graphite and graphene. The π electron cloud surrounds the carbon cage and demonstrates a high level of charge delocalization and conjugation. Beyond those normal molecular orbitals, superatomic molecular orbitals are also found [5–9]. Charge delocalization renders fullerite a strong and fast nonlinear optical response [10, 11], with the third order susceptibility of $\chi^{(3)}$ close to 10^{-12} esu [12]. One naturally expects a strong high harmonic generation (HHG) from C_{60}. Indeed the fifth order harmonic is already observed when one uses a strong laser [13]. In 2005, we predicted a strong HHG from a C_{60} molecule [14–16]. Experimentally, Ganeev *et al.* [17, 18] reported a stronger harmonic signal from C_{60} plasma than from graphite, which is still stronger than that in graphene [19]. However, up to now, there has been no theoretical investigation in solid C_{60}, though investigations in other solids are intensified recently [20–27].

In this Rapid Communication, we carry out a systematic investigation of HHG in solid C_{60}. Solid C_{60} represents the biggest system for HHG, with 60 carbon atoms in the unit cell (see Fig. 1). To handle such a big system, we first use the density functional theory to optimize the C_{60} structure. Since each unit cell has 240 valence electrons, much larger than any prior solids [23], the potential violation of the Pauli exclusion principle is severe, and the single active electron approach is clearly unsuitable. We employ the time dependent Liouville equation for the density matrix, which completely respects the Pauli exclusion principle. The density matrix is used to compute the expectation value of the momentum operator, which is Fourier transformed to the harmonic power spectrum. We employ two different helicities, circularly polarized and linearly polarized laser pulses, with the photon energy from 1.6 to 2.0 eV and pulse duration from 48 to 60 fs. We find that solid C_{60} has a weak helicity dependence due to its high symmetry. The maximum harmonic energy under a moderately strong laser is around 20 eV, in agreement with the experimental results [18].

We find that in general HHG is unable to map the relatively simple band structure of solid C_{60}. However, there is a small window of opportunity if a long wavelength of laser is used. In this case, high order harmonics need multiple photons to lift electrons from the valence to conduction band. In particular, the 5th order harmonics at different crystal momentum $\mathbf{k}$ do not peak at their nominal order; instead a substantial deviation is observed with $\mathbf{k}$, an indication that HHG involves actual band states. When we compare the transition energy dispersion with the harmonic peak energy, we clearly see the hallmark of the band structure. This presents a rare opportunity for HHG. We expect this may motivate future experimental investigation.

Harmonic generation relies on a strong laser pulse. Figure 1 schematically shows an example in solid C_{60}. High harmonics are generated through the intense interaction between the laser and the system. For last thirty years, HHG investigations have focused on atoms and small molecules. Such a spectacular development has overshadowed the earlier work in solids [28] and nanostructures [14]. Farkas *et al.* [28] showed that a picosecond laser pulse can induce HHG from a gold surface. von der Linde *et al.* [29] detected HHG up to the 15th order in an aluminum film and the 14th order in glass where both even and odd harmonics exist. Faisal and Kaminski [30] carried out systematic theoretical investigations in a model thin film and discovered harmonic orders up to 70th. With 5 GW/cm^2 intensity [28], the emitted photon energy is already comparable to the emitted energy in ZnO with TW/cm^2 intensity [23]. Naturally, interests in the solid state HHG are much broader, because it potentially offers a band structure mapping tool [31], but this has not been materialized.

Our first theoretical investigation [14] was based on a tight-binding model in a C_{60} molecule, where all the parameters are tuned to fit the energy band gap and 174 vibrational normal mode frequencies. Although we were limited by the model itself, the results were already very interesting. We found that each harmonic peak can be assigned to a specific transition among molecular orbitals. Our present study employs the first-principles density functional theory as implemented in the Wien2k code [32]. We self-consistently solve the Kohn-Sham equation [32–34],

$$\left[-\frac{\hbar^2\nabla^2}{2m_e} + V_{ne} + V_{ee} + V_{xc}\right]\psi_{n\mathbf{k}}(\mathbf{r}) = E_{n\mathbf{k}}\psi_{n\mathbf{k}}(\mathbf{r}), \tag{1}$$

where m_e is the electron mass, the terms on the left-hand side represent the kinetic energy, nuclear-electron attraction, electron-electron Coulomb repulsion and exchange correlation

[35], respectively. We use the generalized gradient approximation (GGA) at the Perdew, Burke and Ernzerhof (PBE) level [35]. $\psi_{n\mathbf{k}}(\mathbf{r})$ is the Bloch wavefunction of band n at crystal momentum $\mathbf{k}$, and $E_{n\mathbf{k}}$ is the band energy.

Before we compute the harmonic spectrum, we first optimize the solid C_{60} structure. Different from its molecular counterpart, solid C_{60} has several phases, depending on the temperature. In the room temperature, each C_{60} spins rapidly and leads to a disordered phase, with the space group symmetry of $Fm\bar{3}$ (No. 202) [36]. We consider the room temperature phase of solid C_{60} as used in the experiment [17]. We take the experimental lattice constant $a = 14.24$ Å [37], and choose a k mesh of $15 \times 15 \times 15$. The Wien2k code is a full-potential augmented plane wave program. It uses dual basis functions, atomic wavefunctions in the sphere and planewaves in the interstitial region. The product of the Muffin-tin radius R_{MT} and the maximum planewave cutoff K_{max} is 7 (dimensionless) in our study. The optimization proceeds in two steps. First, we reduce R_{MT} by 5% to generate a structure file, so that during the minimization, the Muffin-tin spheres do not overlap. Second, we minimize the total energy with respect to the carbon Wykcoff positions. The entire minimization needs 14 iterations of structural changes, reducing the force on each atom to around 1 mRy/a.u. No further optimization is performed after this step. The final optimized positions are listed in Table I. If we compare them with the experimental positions (see the numbers in parenthesis), we see that the agreement with the experimental results is quite good. Such a good agreement for a large unit cell (60 carbon atoms) demonstrates the accuracy of our first-principles calculation, which is further confirmed by the band structure calculation below.

With the optimized structure in hand, we further compute the transition matrix elements between eigenstates across the Brillouin zone. These transition matrix elements are used for the harmonic generation. We numerically solve the time-dependent Liouville equation for the density matrix ρ [20, 24, 33],

$$i\hbar \frac{\partial \langle n\mathbf{k}|\rho|m\mathbf{k}\rangle}{\partial t} = \langle n\mathbf{k}|[H_0 + H_I, \rho]|m\mathbf{k}\rangle, \tag{2}$$

where $\langle n\mathbf{k}|\rho|m\mathbf{k}\rangle$ is the density matrix element between band states n and m at $\mathbf{k}$ point, H_0 is the field-free Hamiltonian, and H_I is the interaction Hamiltonian between the laser field and C_{60}. Our laser vector potential has two different forms: Circularly polarized light (σ)

and linearly polarized light (π). The circularly polarized light is described by

$$\mathbf{A}(t) = A_0 \mathrm{e}^{-t^2/\tau^2}(\cos(\omega t)\hat{x} \pm \sin(\omega t)\hat{y}), \tag{3}$$

where $\hat{x}$ and $\hat{y}$ are the unit vectors along the x and y axes respectively, t is the time, τ is the laser pulse duration, ω is the carrier frequency, $+$ and $-$ refer to the left (σ^-) and right (σ^+) circularly polarized light within the xy plane, respectively. A_0 is the field amplitude in units of Vfs/Å. One can convert Vfs/Å to V/Å using $E_0(\mathrm{V/Å}) = A_0(\mathrm{Vfs/Å})\omega$, where ω is the laser carrier angular frequency in 1/fs and E_0 is the field amplitude in V/Å. The linearly polarized light has the following form,

$$\mathbf{A}(t) = A_0 \mathrm{e}^{-t^2/\tau^2} \cos(\omega t)\hat{n}, \tag{4}$$

where $\hat{n}$ is the unit vector.

The expectation value of the momentum operator [14, 15] is computed from

$$\mathbf{P}(t) = \sum_{\mathbf{k}} \mathrm{Tr}[\rho_{\mathbf{k}}(t)\hat{\mathbf{P}}_{\mathbf{k}}], \tag{5}$$

where the trace is over band indices and crystal momentum $\mathbf{k}$. The harmonic signal is computed by Fourier transforming $\mathbf{P}(t)$ to frequency domain (see the details in Ref. [20]),

$$\mathbf{P}(\Omega) = \int_{-\infty}^{\infty} \mathbf{P}(t)\mathrm{e}^{i\Omega t}\mathcal{W}(t)dt, \tag{6}$$

where $\mathcal{W}(t)$ is the window function. $\mathcal{W}(t)$ has a hyper-Gaussian shape,

$$\mathcal{W}_1(t) = \exp\left[-(at)^8 \times b\right], \tag{7}$$

where t is the time in fs. a and b are chosen to ensure the interesting regime covered. In our case, we choose $a = 0.035$/fs and $b = 5 \times 10^{-9}$. This window function is necessary since there are very small oscillations at the end of the time evolution. If we do not suppress them, they increase the overall background of the harmonic signal, which smears weak harmonic signals. Our results are not very sensitive to a and b as far as the oscillatory part is dampened out. We should note that using the window function does not affect the magnitude of harmonic signal, which is verified in our actual calculation.

We first choose a left-circularly polarized laser pulse (σ^-) of $\tau = 48$ fs, $\hbar\omega = 1.6$ eV and $A_0 = 0.03$ Vfs/Å. Figure 2(a) shows the results. We see the harmonics reach the 15th

order or about 24 eV, consistent with the experimental results [17]. We also employ a right-circularly polarized laser pulse (σ^+) and the results are similar (see Fig. 2(b)). This lack of helicity dependence of HHG signal is expected from our highly symmetric system. We also polarize our laser polarization along the z axis, instead of the x and y axes alone. Here the signal is only along the z axis. Figure 2(c) shows the harmonics also reach the 15th order. This demonstrates that harmonics are very robust, which explains why Ganeev *et al.* [17] demonstrated a much higher (25 times) harmonic yield than carbon.

The above results only use one photon energy and one pulse duration. We want to see whether different photon energies and durations alter our results. We increase the pulse duration to 60 fs and photon energy to 2 eV. Figure 2(d) shows the results for σ^+. We see that for the same laser field amplitude, the highest harmonic order is reduced to 13, so the maximum harmonic energy is still around 26 eV. We should add that in our calculation, we include all the 120 valence bands (carbon has four valence electrons: $2s^2 2p^2$) from -1.22 Ry and 40 conduction bands up to 0.72 Ry, so the 20-eV plasma excitation is covered. The entire calculation has 120 electrons for each spin channel, and as pointed out by Ganeev *et al.* [17], a single active electron approximation is highly inadequate. Our Liouville formalism handles the Pauli exclusion principle exactly without making any approximation [38] which is not the case in the time-dependent density functional theory. When we use a σ^- pulse, we find the results remain the same (see Fig. 2(e)). This is similar to our results with a pulse of 48 fs and 1.6 eV. We also calculate the harmonic signal along the z axis (Fig. 2(f)) where the maximum order is also at 13.

A particular question is whether one can use HHG as a band probing tool. So far, there is no definitive answer. Vampa *et al.* [31] suggested to use the coherent motion of electron-hole pairs to construct the band structure for ZnO, but it is unclear how general this method is, in particular how one can sample the entire Brillouin zone. We feel that here the theory can make an important contribution. Solid C_{60} has a weak energy dispersion. Fig. 3(a) shows the band structure along the Λ line from the Γ to L point, where the Fermi level E_f is denoted by a horizontal dotted line. The highest occupied molecular orbital (HOMO) and the lowest unoccupied molecular orbital (LUMO) from a single C_{60} molecule form a band for solid C_{60}. Our energy band structure agrees with the prior calculations [39–44]. Theoretically, it is straightforward to compute HHG signals from one $\mathbf{k}$ point at a time, but it is generally unknown whether and what difference the crystal momentum (wave vector)

could make to harmonic generation. This question is important, since if there is no major difference in HHG across different crystal momentum points, then trying to map the band structure by HHG is futile. Theoretical investigation serves an important auxiliary tool to uncover extremely challenging pockets of the Brillouin zone.

The Λ line starts from the Γ point with the full point group symmetry to the L point with symmetry reduced. Our first attempt to get the band structure information is to use a pulse of 60-fs and 2.0-eV, but this does not work. Higher harmonics have a much higher transition energy, so multiple states across several eV contribute the signal, very hard to disentangle them. So we decide to use a smaller photon energy of $\hbar\omega = 0.4$ eV, with $\tau = 60$ fs. The first-order harmonic along the Λ line is shown in Fig. 3(b). Different from Fig. 2 where the harmonic signals are plotted on the logarithmic scale, the **k**-resolved signal is not plotted on the logarithmic scale because the relative difference among different **k** is small in solids. It is clear that the 1st harmonic shows little difference among different **k**, which explains why linear optics has no crystal momentum resolution. The only exception is the Γ point, where the signal is four times weaker than the rest of **k** points. Because of the high symmetry at the Γ point, a direct transition between the HOMO (H_u) and LUMO (T_{1u}) is forbidden due to the parity.

The situation changes at the third harmonic. Figure 3(c) shows that as we move away from the Γ point, there is an immediate uptake in the signal strength. The harmonic signal change is not monotonic: It decreases first with **k**, and when we are closer to the L point, there is a small increase. The inset of Fig. 3(c) shows the dispersion of the harmonic signal with **k**. This result answers the above important question. If one detects the signal along these crystal momentum directions, one indeed can probe the band dispersion in terms of transition amplitude through the harmonic signal change. A theoretically guided probe is amenable to future experiments.

To probe an energy dispersion, we move to the 5th harmonic (Fig. 3(d)). While its peak amplitude drops by two orders of magnitude, in comparison with the third order, the energy dispersion manifests itself through the peak energy shift. The peak at Γ does not appear at its nominal order of 5 (i. e. $5\hbar\omega = 2.0$ eV), and instead now appears at 2.05 eV, close to the transition energy of 2.44 eV between the HOMO and LUMO+1 states. Shifting away from the nominal harmonic order is an indication that band energy states participate in HHG through real excitation, which is already clear in the C_{60} molecule [14]. Therefore, it is

instructive to examine whether the peak energy matches the transition energy ΔE between the valence and conduction bands.

Since the lowest transition is dipole-forbidden, we look at the second lowest transition between the H_u band and T_{1g} band. A true band mapping should show that the transition energy follows the harmonic peak energy closely. Figure 4 compares the fifth harmonic peak energy and ΔE. We see that ΔE (empty circles) is quite smooth and flat, lying between 2.4 and 2.5 eV. The harmonic peak energy (empty boxes), around 2.0 eV, decreases slightly up to Λ_3, then increases and eventually saturates around 2 eV. Since at the Λ_5 point the harmonic intensity is too weak, we do not include it in our figure. So our conclusion is mixed. HHG indeed has the potential to map the band structure. However, a good match is not found in solid C_{60}. In general, we expect that the flat band structure should be ideal for HHG, but because harmonic generation involves the transition matrix elements, just like photoemission, harmonic peak energies are undoubtedly affected by transition matrix elements. One possible solution is to fine tune the photon energy, but then this is not a generic method since experimentally tuning photon energy is not easy.

In conclusion, we have investigated high harmonic generation in solid C_{60} for the first time at the first-principles density functional level. A particular challenge for solid C_{60} is that at each crystal momentum point 240 valence electrons participate laser-induced excitation, far beyond the single-active electron approach often used in HHG calculations for atoms and small molecules. Instead, we employ the Liouville equation of density matrices which respects the Pauli exclusion rigorously, in contrast to the time-dependent density functional theory. We show that C_{60} generates harmonics all the way to up to 15 with a moderately strong laser pulse, which agrees with the prior experiment from C_{60} plasma [17]. Due to the high spherical symmetry, harmonic signals show a weak dependence on the laser helicity. Increasing the photon energy from 1.6 to 2.0 eV, we observe a reduction of harmonic order, which indicates there is a maximum harmonic energy around 20 eV. This 20 eV matches the well known plasma resonance. Solid C_{60} has a weak band dispersion, which is ideal for band mapping [31], but our results show that there is no big difference in HHG among different crystal momenta in general. However, if we choose a photon energy that is much smaller than the minimum energy gap of dipole-allowed transitions between the valence and conduction bands, higher order harmonics show a clear dispersion. This represents an opportunity for future experimental investigation.

Acknowledgments

This work was solely supported by the U.S. Department of Energy under Contract No. DE-FG02-06ER46304. Part of the work was done on Indiana State University's high performance Quantum and Obsidian clusters. The research used resources of the National Energy Research Scientific Computing Center, which is supported by the Office of Science of the U.S. Department of Energy under Contract No. DE-AC02-05CH11231.

* guo-ping.zhang@outlook.com

---

[1] H. W. Kroto, J. R. Heath, S. C. O'Brien, R. F. Curl, and R. E. Smalley, C_{60}: Buckminsterfullerene, Nature **318**, 162 (1985).

[2] J. E. Fischer, P. A. Heiney, A. R. McGhie, W. J. Romanow, A. M. Denenstein, J. P. McCauley Jr., and A. B. Smith III, Compressibility of Solid C_{60}, Science **252**, 1288 (1991).

[3] A. F. Hebard, M. J. Rosseinsky, R. C. Haddon, D. W. Murphy, S. H. Glarum, T. T. M. Palstra, A. P. Ramirez, and A. R. Kortan, Superconductivity at 18 K in potassium-doped C_{60}, Nature **350**, 600 (1991).

[4] M. Mitrano, A. Cantaluppi, D. Nicoletti, S. Kaiser, A. Perucchi, S. Lupi, P. Di Pietro, D. Pontiroli, M. Ricc, S. R. Clark, D. Jaksch, and A. Cavalleri, Possible light-induced superconductivity in K_3C_{60} at high temperature, Nature **530**, 461 (2016).

[5] M. Feng, J. Zhao and H. Petek, Atomlike, hollow-core-bound-molecular orbitals of C_{60}, Science **320**, 359 (2008).

[6] J. Zhao, M. Feng, J. Yang, and H. Petek, The superatom states of fullerenes and their hybridization into the nearly free electron bands of fullerites, ACS Nano **3**, 853 (2009).

[7] G. J. Dutton, D. B. Dougherty, W. Jin, J. E. Reutt-Robey, and S. W. Robey, Superatom orbitals of C_{60} on Ag(111): Two-photon photoemission and scanning tunneling spectroscopy, Phys. Rev. B **84**, 195435 (2011).

[8] G. P. Zhang, H. P. Zhu, Y. H. Bai, J. Bonacum, X. S. Wu, and T. F. George, Imaging superatomic molecular orbitals in a C_{60} molecule through four 800-nm photons, International Journal of Modern Physics B **29**, 1550115 (2015).

[9] G. P. Zhang, A. Gardner, T. Latta, K. Drake, and Y. H. Bai, Superintermolecular orbitals in

the C_{60}-pentacene complex, Phys. Rev. A **94**, 062501 (2016).

[10] Z. H. Kafafi, J. R. Lindle, R. G. S. Pong, F. J. Bartoli, L. J. Lingg, and J. Milliken, Off-resonant nonlinear optical properties of C_{60} studied by degenerate four-wave mixing, Chem. Phys. Lett. **188**, 492 (1992).

[11] S. L. Dexheimer, D. M. Mittleman, R. W. Schoenlein, W. Vareka, X.-D. Xiang, A. Zettl, and C. V. Shank, Ultrafast Dynamics of Photoexcited C_{60}, in *Ultrafast Pulse Generation and Spectroscopy*, edited by T. R. Gosnell, A. J. Taylor, K. A. Nelson, and M. C. Downer, SPIE Proc. **1861**, 328 (1993).

[12] S. R. Flom, R. G. S. Pong, F. J. Bartoli, and Z. H. Kafafi, Resonant nonlinear optical response of the fullerenes C_{60} and C_{70}, Phys. Rev. B **46**, 15598 (1992).

[13] J. R. Lindle, R. G. S. Pong, F. J. Bartoli, and Z. H. Kafafi, Nonlinear optical properties of the fullerenes C_{60} and C_{70} at 1.064 μm, Phys. Rev. B **48**, 9447 (1993).

[14] G. P. Zhang, Optical high harmonic generations in C_{60}, Phys. Rev. Lett. **95**, 047401 (2005).

[15] G. P. Zhang and T. F. George, Ellipticity dependence of optical harmonic generation in C_{60}, Phys. Rev. A **74**, 023811 (2006).

[16] G. P. Zhang and T. F. George, Origin of ellipticity anomaly in harmonic generation in C_{60}, J. Optical Society of America B **24**, 1150 (2007).

[17] R. Ganeev, L. Bom, J. Abdul-Hadi, M. Wong, J. Brichta, V. Bhardwaj, and T. Ozaki, Higher-order harmonic generation from fullerene by means of the plasma harmonic method, Phys. Rev. Lett. **102**, 013903 (2009).

[18] R. Ganeev, L. E. Bom, M. C. H. Wong, J.-P. Brichta, V. Bhardwaj, P. Redkin, and T. Ozaki, High-order harmonic generation from C_{60}-rich plasma, Phys. Rev. A **80**, 043808 (2009).

[19] N. Yoshikawa, T. Tamaya, and K. Tanaka, High-harmonic generation in graphene enhanced by elliptically polarized light excitation, Science **356**, 736 (2017).

[20] G. P. Zhang, M. S. Si, M. Murakami, Y. H. Bai, and T. F. George, Generating high-order optical and spin harmonics from ferromagnetic monolayers, Nat. Commun. **9**, 3031 (2018).

[21] T. Higuchi, M. I. Stockman and P. Hommelhoff, Stron-field perspective on high-harmonic radiation from bulk solids, Phys. Rev. Lett. **113**, 213901 (2014).

[22] N. Tancogne-Dejean, M. A. Sentef, and A. Rubio, Ultrafast modification of Hubbard U in a strongly correlated material: *ab initio* high-harmonic generation in NiO, Phys. Rev. Lett. **121**, 097402 (2018).

[23] S. Ghimire, E. Sistrunk, P. Agostini, L. F. DiMauro, and D. A. Reis, Observation of high-order harmonic generation in a bulk crystal, Nat. Phys. **7**, 138 (2011).

[24] G. P. Zhang and Y. H. Bai, Magic high-order harmonics from a quasi-one-dimensional hexagonal solid, Phys. Rev. B **99**, 094313 (2019).

[25] L. Jia, Z. Zhang, D. Z. Yang, M. S. Si, G. P. Zhang, and Y. S. Liu, High harmonic generation in magnetically-doped topological insulators, Phys. Rev. B **100**, 125144 (2019).

[26] H. K. Avetissian, A. K. Avetissian, B. R. Avchyan and G. F. Mkrtchian, Multiphoton excitation and high-harmonic generation in topological insulator, J. Phys.: Condens. Matter **30** 185302 (2018).

[27] H. K. Avetissian and G. F. Mkrtchian, Impact of electron-electron Coulomb interaction on the high harmonic generation process in graphene, Phys. Rev. B **97**, 115454 (2018).

[28] Gy. Farkas, Cs. Tóth, S. D. Moustaizis, N. A. Papadogiannis, and C. Fotakis, Observation of multiple-harmonic radiation induced from a gold surface by picosecond neodymium-doped yttrium aluminum garnet laser pulses, Phys. Rev. A **46**, R3605 (1992).

[29] D. von der Linde, T. Engers, G. Jenke, P. Agostini, G. Grillon, E. Nibbering, A. Mysyrowicz and A. Antonetti, Generation of high-order harmonics from solid surfaces by intense femtosecond laser pulses, Phys. Rev. A **52**, R25 (1995).

[30] F. H. M. Faisal and J. Z. Kamiński, Generation and control of high harmonics by laser interaction with transmission electrons in a thin crystal, Phys. Rev. A **54**, R1769 (1996).

[31] G. Vampa, T. J. Hammond, N. Thire, B. E. Schmidt, F. Legare, C. R. McDonald, T. Brabec, D. D. Klug, and P. B. Corkum, All-optical reconstruction of crystal band structure, Phys. Rev. Lett. **115**, 193603 (2015).

[32] P. Blaha, K. Schwarz, G. K. H. Madsen, D. Kvasnicka, and J. Luitz, WIEN2k, An Augmented Plane Wave + Local Orbitals Program for Calculating Crystal Properties (Karlheinz Schwarz, Techn. Universität Wien, Austria, 2001).

[33] G. P. Zhang, W. Hübner, G. Lefkidis, Y. Bai, and T. F. George, Paradigm of the time-resolved magneto-optical Kerr effect for femtosecond magnetism, Nat. Phys. **5**, 499 (2009).

[34] G. P. Zhang, Y. H. Bai, and T. F. George, Energy- and crystal momentum-resolved study of laser-induced femtosecond magnetism, Phys. Rev. B **80**, 214415 (2009).

[35] J. P. Perdew, K. Burke, and M. Ernzerhof, Generalized gradient approximation made simple, Phys. Rev. Lett. **77**, 3865 (1996).

[36] W. I. F. David, R. M. Ibberson, J. C. Matthewman, K. Prassides, T. John S. Dennis, J. P. Hare, H. W. Kroto, R. Taylor, and D. R. M. Walton, Crystal structure and bonding of ordered C_{60}, Nature **353**, 147(1991).

[37] D. L. Dorset and M. P. McCourt, Disorder and the molecular packing of C_{60} buckminsterfullerene: a direct electron-crystallographic analysis, Acta Crystallographica A **50**, 344 (1994).

[38] G. P. Zhang, Y. H. Bai, and T. F. George, Ultrafast reduction of exchange splitting in ferromagnetic nickel, J. Phys.: Condens. Mat. **28**, 236004 (2016).

[39] Y. N. Xu, M. Z. Huang, and W. Y. Ching, Optical properties of superconducting K_3C_{60} and insulating K_6C_{60}, Phys. Rev. B **44**, 13171 (1991).

[40] S. Saito and A. Oshiyama, Cohesive mechanims and energy bands of solid C_{60}, Phys. Rev. Lett. **66**, 2637 (1991).

[41] W. Y. Ching, M. Z. Huang, Y. N. Xu, W. G. Harter, and F. T. Chan, First-principles calculation of optical properties of C_{60} in the fcc lattice, Phys. Rev. Lett. **67**, 2045 (1991).

[42] N. Troullier and J. L. Martins, Structural and electronic properties of C_{60}, Phys. Rev. B **46**, 1754 (1992).

[43] S. C. Erwin, Electronic structure of the alkali-intercalated fullerides, endohedral fullerenes, and metal-adsorbed fullerenes, in *Buckminsterfullerenes*, edited by W.E. Billups and M.A. Ciufolini (VCH, New York), p. 217 (1993).

[44] E. L. Shirley and S. G. Louie, Electronic excitations in solid C_{60}: Energy gap, band dispersions, and effects of orientational disorder, Phys. Rev. Lett. **71**, 133 (1993).

TABLE I: Theoretically optimized Wykcoff positions for solid C_{60}. Numbers in parentheses are experimental ones [37]. The experimental lattice constant is $a = b = c = 14.26$ Å at room temperature, where C_{60} is disordered and the solid C_{60} has $Fm\bar{3}$ symmetry, No. 202. In our optimization, we use the experimental lattice constant.

Atom	x		y		z	
	Theory	Experiment	Theory	Experiment	Theory	Experiment
C_1	0.04913	(0.052)	0	(0)	0.24451	(0.249)
C_2	0.09995	(0.105)	0.08228	(0.085)	0.21267	(0.220)
C_3	0.18222	(0.185)	0.05085	(0.052)	0.16153	(0.165)

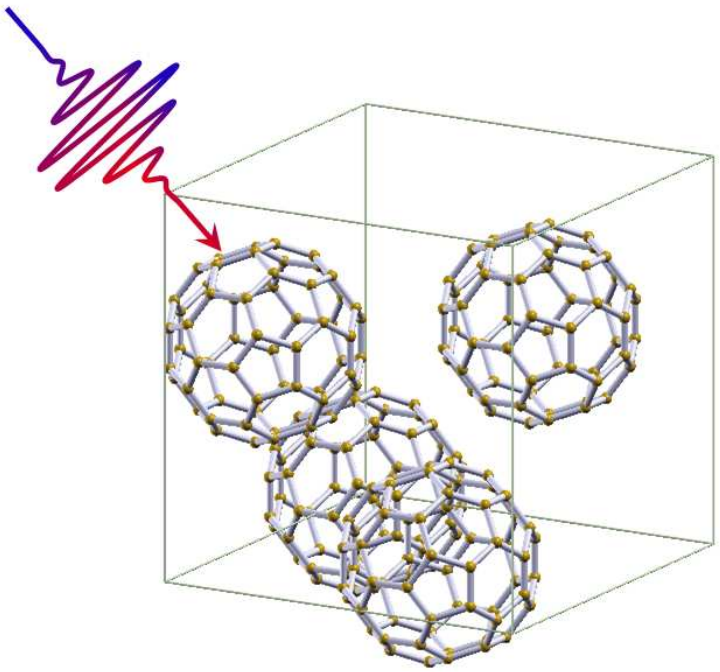

FIG. 1: High harmonic generation in solid C_{60}. After a fs laser pulse impinges on to C_{60}, high order harmonics are generated. Solid C_{60} crystallizes to an fcc structure at room temperature.

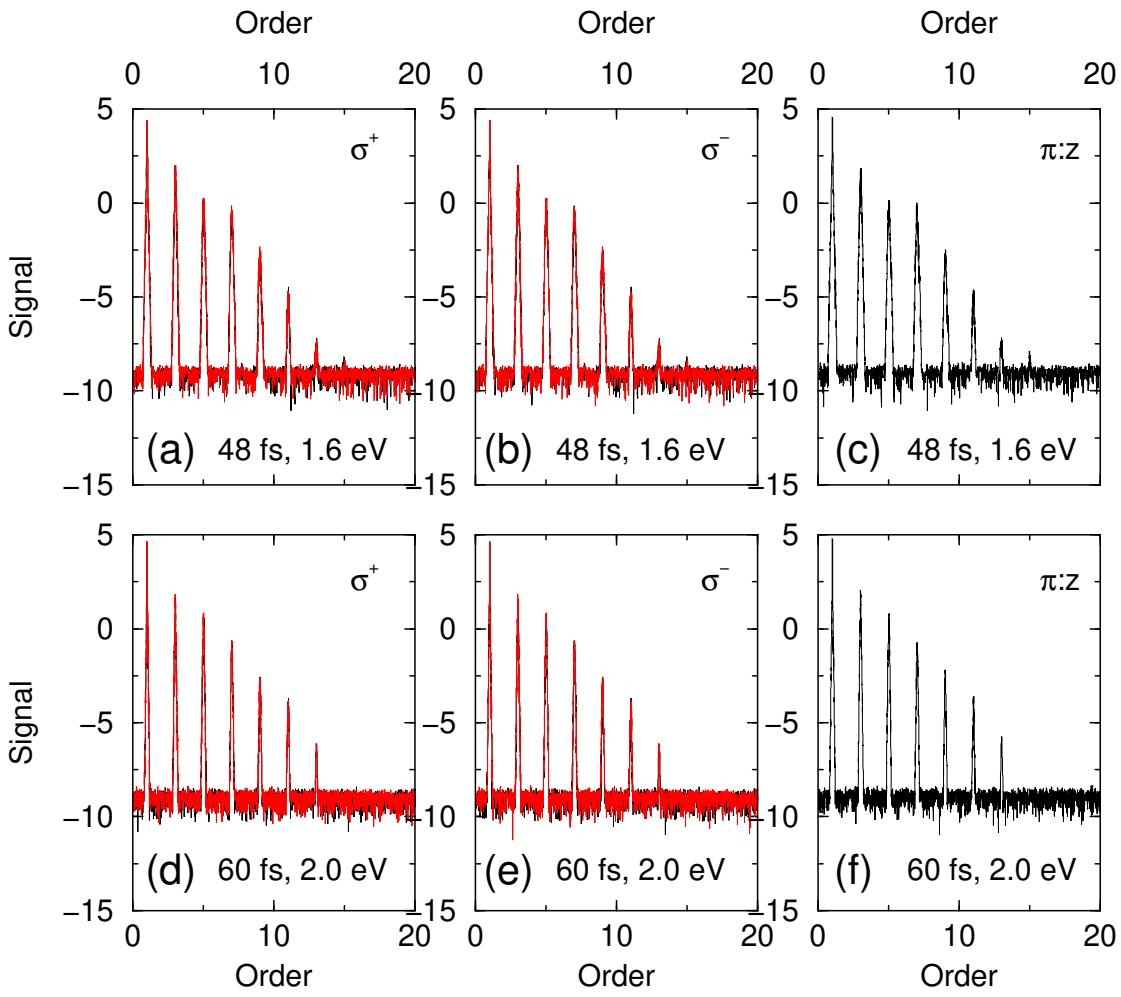

FIG. 2: High harmonic generation from solid C_{60} under different laser configurations. The signal is plotted on the logarithmic scale. (a) Right-circularly polarized light (σ^+) within the xy plane. The photon energy is $\hbar\omega = 1.6$ eV, the duration is $\tau = 48$ fs, and the laser field amplitude is $A_0 = 0.03$ Vfs/Å. (b) Left-circularly polarized light (σ^-) within the xy plane. Other parameters are the same as (a). (c) Linearly polarized light (π) along the z direction. Other parameters are the same as (a). (d) Right-circularly polarized light (σ^+) within the xy plane. The photon energy is $\hbar\omega = 2.0$ eV, the duration is $\tau = 60$ fs, and the laser field amplitude is $A_0 = 0.03$ Vfs/Å. (e) Left-circularly polarized light (σ^-) within the xy plane. Other parameters are the same as (d). (f) Linearly polarized light (π) along the z direction. Other parameters are the same as (d).

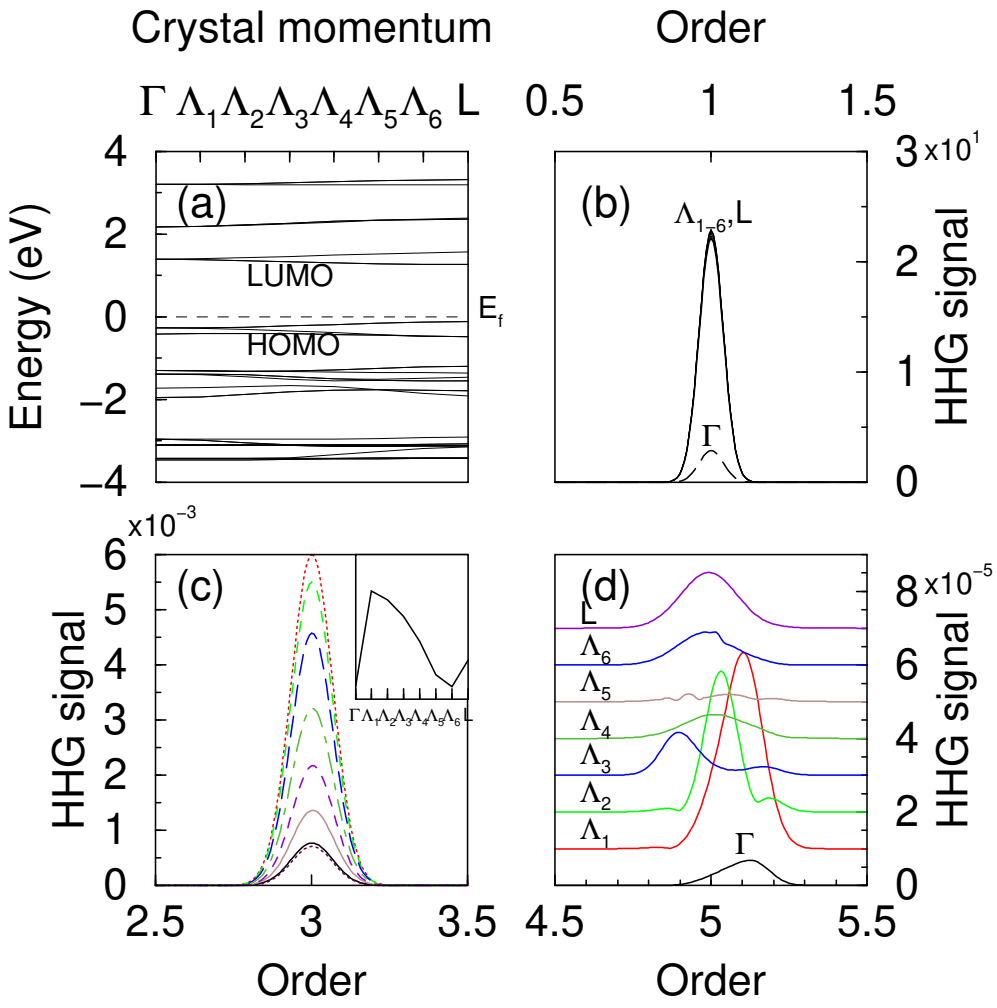

FIG. 3: (a) Energy band dispersion along the Λ line from the Γ to L point. (b) The first harmonic is resolved along the Λ line. Here and below harmonic signals are plotted in their natural unit. The laser field amplitude is 0.03 Vfs/Å, the photon energy is $\hbar\omega = 0.4$ eV, the pulse duration is $\tau = 60$ fs, and the linearly polarized light along the z axis is used. The first order harmonic has no big difference among different $\mathbf{k}$ points. The weakest signal is at the Γ point. (c) The third harmonic is plotted along the Λ line. The amplitude change is plotted in the inset, where a clear dispersion is noted. (d) The fifth harmonic shows a stronger dispersion. Both the harmonic signal strength and the peak position disperse strongly with $\mathbf{k}$. All the curves, except the one at Γ, are vertically shifted for clarity.

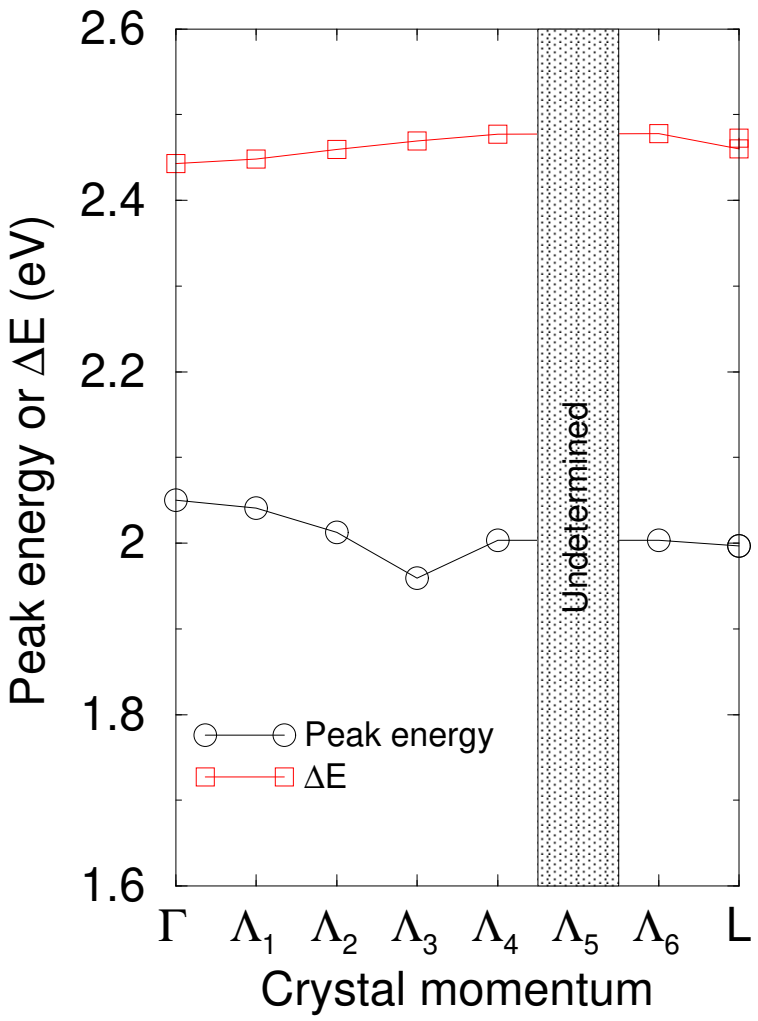

FIG. 4: Comparison between the harmonic peak energy of the fifth harmonic (the empty circles) and transition energy ΔE (the empty boxes) from the H_u band to T_{1g} band. At the Λ_5, the harmonic signal is too weak, so it is not plotted.